Wood Science and Technology (2022) 56:1029–1045
https://doi.org/10.1007/s00226-022-01394-x

ORIGINAL

# Large-scale and high-resolution visualization of static mechanical properties of wood-adhesive interphase utilizing nanoindentation mapping

**Chuhang Xu[1] · Yizhong Cao[1,2] · Haili Chen[1,2] · Yujing Nie[1,2] · Yujie Meng[3] · Qiang Wu[1,2] · Siqun Wang[4]**

Received: 9 November 2021 / Accepted: 30 May 2022 / Published online: 21 June 2022


## Abstract

To improve the mechanical performance of wooden engineered composites, more information is needed to understand the relationship between adhesive infiltration and mechanical properties of wood-adhesive interphase. Nanoindentation mapping (NI Mapping) was hereby used to achieve large-scale and high-resolution visualization of mechanical properties of wood-adhesive interphase for establishing the basic understanding of such correlation, and it showed the convincible reliability (variation less than 3% as compared with commonly applied NI methodology) and exceptional efficiency (180 min of total analysis time as compared with more than 3000 min using the commonly applied NI methodology). Successful investigation into the distribution of mechanical properties of wood-phenolic resin (wood-PF) and wood-polyurethane (wood-PUR) interphases using NI Mapping has confirmed that gradient elevation in mechanical properties of cell wall in wood-adhesive interphase is related to adhesive infiltration. PF adhesive exhibits favored infiltration which led to the enlarged wood-PF interphase region (over 60 μm) and improved micro-/macro-mechanical properties. NI Mapping was also applied for revealing mechanical performance of early wood-adhesive interphase which cannot be characterized by commonly applied NI methodology due to its small size. The mechanical properties of cell wall in early wood-adhesive interphase are poor; however, the interphase region would be enlarged due to the large lumen of early wood. NI Mapping can be a powerful tool to provide significant insights into the mechanical properties of wood-adhesive interphase, and thus, to improve the knowledge of the adhesive infiltration and mechanical properties of cell wall.

✉ Yizhong Cao
20210024@zafu.edu.cn

✉ Qiang Wu
wuqiang@zafu.edu.cn

Extended author information available on the last page of the article

## Introduction

Wooden engineered composites, including laminated veneer lumber (LVL), oriented strand board (OSB), and cross laminated timber (CLT), have been widely applied to civil wooden architecture due to the great strength-weight ratio and exceptional environmental conservation as compared with steel and cement (Aicher et al. 2016, Yu et al. 2017). As the application of wooden engineered composites has increased, their mechanical properties have attracted continuous attention. It is attributed to the fact that its mechanical properties can significantly affect the service life and the safety of civil wooden architecture. Previous research pinpointed that the mechanical properties of wooden engineered composites are highly contingent on the structure and mechanical properties of the wood-adhesive interphase (Kamke 2007; Frihart 2013). It has been demonstrated that the wood-adhesive interphase plays an important role in strain and stress transfer when the wooden engineered composite bears load (Baldan 2012). Continuous attention has thus been paid to revealing the structures and mechanical properties of the wood-adhesive interphase, which is of great significance to optimize wooden engineered composites. One important issue is to know the correlation between the adhesive infiltration and mechanical properties of the wood-adhesive interphase.

In recent years, methodologies based on laser scanning confocal microscopy (Gavrilovic-Grmusa et al. 2012; Altgen et al. 2019), electron microscopy (Singh et al. 2015), X-ray computed tomography (XCT) (Kamke et al. 2014; McKinley et al. 2018; Jakes et al. 2019) and infrared nano-spectroscopy (Wang et al. 2016, 2018b) were used to reveal the adhesive infiltration in the wood-adhesive interphase. It has been demonstrated that the adhesive can infiltrate into the cell wall, and the interpenetrating polymer networks (IPNs) between adhesive and cell wall skeleton can be formed accordingly (Jakes et al. 2015). Aforementioned studies revealed that the infiltration of adhesive into wood substrate may elevate the mechanical properties of the wood-adhesive interphase by forming close-knit IPNs and improving the density of wood cell wall. Researchers also used nanoindentation (NI) analyses to directly measure the mechanical properties of the wood-adhesive interphase. Using suitable NI methodologies can demonstrate the static mechanical properties (including elastic modulus and hardness) (Konnerth et al. 2006; Herzele et al. 2018), yielding strength (Zhang et al. 2010) and creep behaviors (Zhang et al. 2012; Wang et al. 2018a) of the wood-adhesive interphase. NI analyses can also be used to evaluate the adhesion between adhesive and wood cell wall using adhesion energy as the indicator (Obersriebnig et al. 2012, 2013).

NI analyses exhibit promising advantages for providing significant insights into the mechanical properties of wood-adhesive interphase. Yet, it also faces obstacles for revealing the correlation between adhesive infiltration and mechanical properties of the wood-adhesive interphase. NI methodology depends on discrete indents to reflect the mechanical properties of the wood-adhesive interphase. Due to the hierarchical structure and complex anatomical characteristics of wood,

the infiltration of adhesive into wood substrate is uneven, which further causes the variation in mechanical properties of the wood-adhesive interphase (Kamke 2007; Baldan 2012). To reflect the mechanical properties of wood-adhesive interphase in large scale, large numbers of indents need to be conducted, inducing time-consuming analysis. The NI methodology depending on matrix-arrayed indents has now been applied to reveal the variations in the mechanical properties of the interphase in plant fiber reinforced composites (Li et al. 2017; Zhang et al. 2020). However, the NI methodology still exhibited limitations with respect to evaluation scale ($20 \times 30$ μm$^2$) and numbers of indents ($5 \times 15$ indents). Thus, obtained cartographies of elastic modulus and hardness were of relatively low-resolution. To deepen the understanding of the adhesive infiltration and the distribution of mechanical properties in the wood-adhesive interphase, it is desired to achieve large-scale and high-resolution visualization of mechanical properties in the wood-adhesive interphase.

Recently, Wu et al. (2021) successfully applied a new NI methodology (NI Mapping) to reveal the mechanical properties of wood-coating interphase. Benefiting from NI Mapping, $100 \times 100$ indents can be performed in an area of $100 \times 100$ μm$^2$, thus elevating the resolution of obtained cartographies of mechanical properties. In terms of investigating the wood-adhesive interphase in a large scale, both XCT and NI Mapping exhibit obvious advantages, which however aim for different goals. An apparent advantage of XCT is that it can provide a visual 3D segmented volume that displays the infiltration of adhesive (Jakes et al. 2019). Moreover, the detection scale of XCT reaches up to millimeter-level with a sub-micro resolution, which undeniably caves a way for precise study of adhesive infiltration into wooden substrates (Evans et al. 2010; Beaulieu et al. 2019; Szewczykowski et al. 2019). In conjunction with the built-in shearing/bending instruments, XCT can provide information on the deformation process of materials (including the fracture and strain rate) (Zauner et al. 2012; Huang et al. 2015; Kutukova et al. 2018; Qi et al. 2020). However, XCT cannot provide the mechanical properties of cell wall or adhesive. As NI Mapping can investigate the mechanical properties of wood-adhesive interphase, it exhibits advantages compared to XCT.

The objective of this study is using NI Mapping to achieve the large-scale and high-resolution visualization of mechanical properties in the wood-adhesive interphase, i.e., revealing the correlation between adhesive infiltration and mechanical properties of wood-adhesive interphase. The mechanical properties in the early wood-adhesive interphase were also studied using NI Mapping. The obtained results can enrich the knowledge of mechanical properties of the wood-adhesive interphase, and be beneficial to improve the design of the wood-adhesive interphase.

## Materials and methods

### Materials

All involved wood blocks ($3 \times 3 \times 15$ mm$^3$) were cut from the same defect-free section of Douglas fir (*Pseudotsuga menziesii)*. The moisture content of wood blocks

was adjusted to 6% prior to further adhesion. Two typical adhesives were applied to manufacture the wooden engineered composites, i.e., phenol–formaldehyde adhesive (PF) and one-component polyurethane adhesive (PUR). The viscosity of PF resin as measured at 25 °C was 150 mPa·s and the solid content corresponded to 45.6%. The viscosity of PUR as measured at 25 °C was 300 mPa·s, and the corresponding solid content was 99.1%. Both PF and PUR used in this work were purchased from the Dare wood-based composites Group, China and the adhesives were used as received.

### Wood-adhesive bonds preparation

Selected wood blocks were bonded using PF and PUR, respectively. PF/PUR adhesive was applied on the radial section of Douglas fir with an adhesive consumption of 150 $g{\cdot}m^{-2}$. In this way, the adhesive infiltrated into the wood along the tangential direction. After the adhesive was applied, the PF-wood bonds went through a hot-press procedure at 0.8 MPa and 140 °C for 40 min. The PUR-wood bonds went through a similar procedure at 25 °C. After that, all wood-adhesive bonds were kept at 25 °C and 55% (relative humidity) for 48 h to relieve the inner stress induced by curing of adhesive.

### Shear strength of wood-adhesive bonds

The shear strength of wood-adhesive bonds was evaluated according to the Chinese National Standard (GB/T 17657 -2013) using a universal mechanical testing machine (Instron 3400, USA). 12 replicates were performed. The fracture of early wood-adhesive interphase was investigated using an ultra-field depth optical microscope (VHX-500, Keyence, China).

### NI sample preparation

The methodology reported in previous research was applied to prepare the sample for NI analyses (Jakes et al. 2008). An ultra-microtome (Leica MZ6, Germany) equipped with a diamond knife was used to prepare smooth surfaces on the cross section of the prepared wood-adhesive bonds prior to NI analyses. To avoid the influence of the embedding agents, the samples were prepared without embedding procedures. The temperature and relative humidity of NI chamber were controlled at 25 °C and 55%, respectively. All samples were conditioned to a uniform moisture content of 8% after hot-pressing and they were placed in NI chamber for 24 h to minimize any undesired dimensional changes or thermal expansion.

### NI Mapping

iMicro nanoindenter (KLA, USA) equipped with a Berkovich indenter was used to achieve large-scale and high-resolution visualization of mechanical properties in the wood-adhesive interphase. The NI Mapping methodology (NanoBlitz

3D) is integrated in the cluster of NI methodologies of the software. The NI Mapping proposed in this work was performed in continuous stiffness measurement (CSM) mode, i.e., all mapping indents were performed in the CSM mode. The testing depth of single indent was determined in the same CSM mode and the results (Fig. 1) revealed that the elastic modulus and hardness of the cell wall, corner compound middle lamella (CCML) and PF adhesive were relatively constant (variance less than 10%) as the indent depth exceeded 180 nm. Thus, the testing depth of all indents in NI Mapping was set as 200 nm. The elastic modulus and hardness of indents in NI Mapping were the average of the results obtained from the depth range of 180–200 nm. Each indentation was performed to a specified depth of 200 nm, so that a spacing of 1 μm between indentations could be used while still ensuring an indentation depth/spacing ratio of ≈ 5 was maintained according to previous research (Cao et al. 2021). Each indentation was conducted in ≈ 1 s with an oscillation amplitude of 5 nm and a frequency of 110 Hz.

Figure 1 a3–c3 displays the representative load-depth curves of S2 layer of cell wall, adhesive-infiltrated CCML and PF adhesive. The obvious advantage of CSM mode used here is that it allows the measurement of contact stiffness at any point along the loading curve and not just at the point of unloading when compared to the conventional measurement (Li et al. 2002). Another advantage in CSM mode is that it can significantly reduce the time required for calibration and testing procedures (Oliver et al. 2004). Hereby, the contact stiffness was obtained at a point in unloading segment where 95% load remained. In this work, the mechanical properties obtained from NI Mapping were used as relative values to reveal the correlation

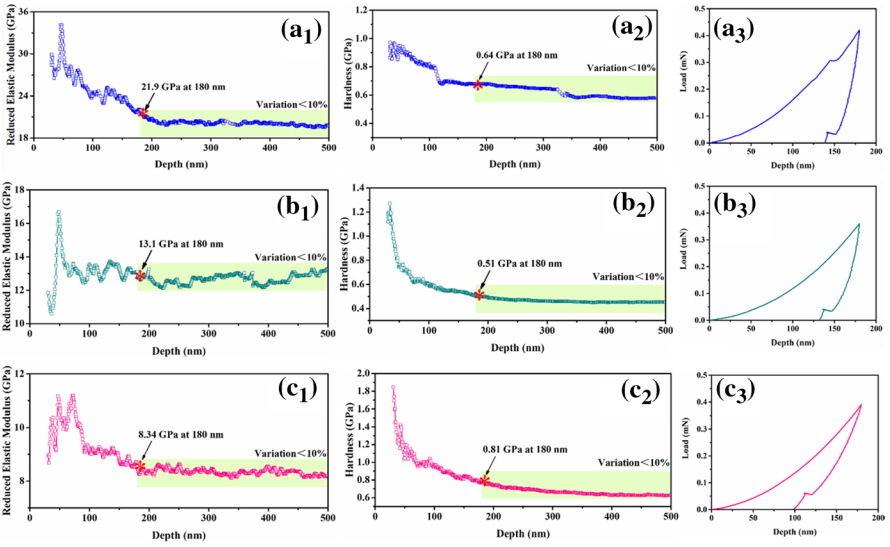


**Fig. 1** Elastic modulus and hardness of ($\mathbf{a_1}$, $\mathbf{a_2}$) S2 layer of cell wall, ($\mathbf{b_1}$, $\mathbf{b_2}$) adhesive-infiltrated corner compound middle lamella (CCML) and ($\mathbf{c_1}$, $\mathbf{c_2}$) PF adhesive as a function of testing depth. ($\mathbf{a_3}$–$\mathbf{c_3}$) Representative load-depth curves corresponding to S2 layer of cell wall, adhesive-infiltrated CCML and PF adhesive, respectively

between adhesive infiltration and mechanical properties of cell wall in wood-adhesive interphase, which is the major objective of this work.

As shown in Fig. 2a and b, the area of interest (AOI) was chosen at wood-adhesive interphase with a dimension of 100 × 100 μm$^2$. 100 × 100 indents were performed in an array within AOI. The reduced elastic modulus ($E_r$) and hardness ($H$) corresponding to each indent can be calculated according to the following method (Oliver et al. 1992):

$$E_r = \frac{\sqrt{\pi}}{2\beta}\frac{S}{\sqrt{A}} \tag{1}$$

$$H = \frac{P_{\max}}{A} \tag{2}$$

In Eq. 1, S refers to the initial unloading stiffness, β corresponds to a correction factor which is correlated to the indenter's geometry ($\beta = 1.034$ for a Berkovich indenter), and A refers to the projected contact area at peak load. In Eq. 2, $P_{\max}$ refers to the peak load of indent.

In this work, the verified nanoindentation tests were performed on the area that is adjacent to the AOI in the same wood-adhesive interphase as shown in Fig. 2a. 12 verified indents were performed on the cell wall S2 layer and CCML using the commonly applied NI methodology (max load of 0.4 mN, loading in 5 s, holding load for 5 s and unloading in 5 s), respectively (Konnerth 2014; Wang et al. 2017a). The $E_r$ and $H$ obtained from verified indents were calculated according to Eqs. 1 and 2. The obtained data was averaged and compared with

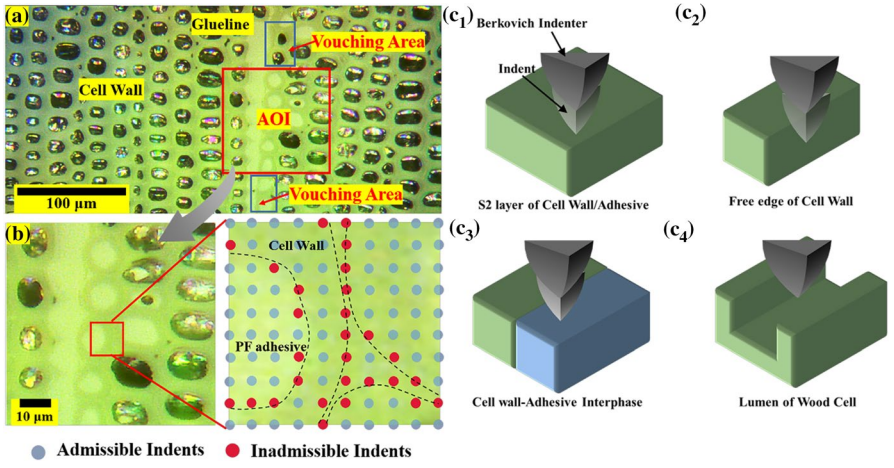


**Fig. 2** **a** Optical image of a wood-PF interphase. The AOI (100 × 100 μm$^2$) and vouching area are displayed. **b** Enlarged optical image of AOI and a representative array with 10 × 10 indents are displayed. **(c1–c4)** Four types of indenter locations. Results obtained from c1 were applied to subsequent analyses and results obtained from c4 were automatically 0

the one obtained from NI Mapping at the similar locations. For comparison, the data sets (approximately 120 data) corresponding to similar locations were separated from the cartography of NI Mapping and then averaged.

The cartographies of reduced elastic modulus and hardness were generated based on the high throughput data obtained from NI Mapping. Origin 2016 was used for data analysis, and the median filtering was applied to the interpolation to form a continuous mapping during plotting. As displayed in Figure S1 (*Supporting Information*), the interpolated data was only used for the continuous mapping and was excluded from any subsequent analyses. In Fig. 2b, the grid of indents covered the AOI with a total $100 \times 100$ indents and a space of indents of 1 μm. Indents can locate in S2 layer of cell wall/adhesive (Fig. 2c1), free edge of cell wall (Fig. 2c2), cell wall-adhesive interphase (Fig. 2c3) and the lumen of wood cell (Fig. 2c4). As pinpointed by Jakes et al. (2008), the structural compliances of the situations like Fig. 2c2 and c3 are massive and could lead to obvious error in the obtained data (Jakes et al. 2008). In addition, the indents located in aforementioned locations violated the assumption of the Oliver-Pharr method (flat, isotropous and semi-finite materials). Therefore, such data cannot be analyzed. In this work, a principle was adopted for selection and analysis of the results of NI Mapping. As displayed in Fig. 2b, indents that violated the basic assumption of Oliver-Pharr method were excluded for subsequent analyses, only indents located in the cell wall S2 layer and CCML were used. After generating the cartography of elastic modulus and hardness, the corresponding data was excluded from subsequent analyses via a careful verification. For the locations in the lumen of the wood cell, the Berkovich indenter cannot detect loading within the displacement (0–200 nm). Thus, the corresponding data is automatically measured as 0.

## Results and discussion

### Reliability of NI Mapping

For verifying the reliability of NI Mapping, the elastic modulus and hardness of chosen areas were compared using NI Mapping and commonly applied NI methodology (Fig. 3). It should be noted that the adhesive infiltration resulted in the elevated mechanical properties of adhesive-infiltrated CCML as compared with the one without adhesive infiltration as reported in previous literature (Wimmer et al. 1997; Jakes et al. 2021; Phani et al. 2021). The variance between the mechanical properties obtained from different NI methodologies is less than 3.0%. The Berkovich indenter used in this work is a self-similar probe which could result in independent results with the load added (Li et al. 2020). Therefore, it can be concluded that the mechanical properties of the wood-adhesive interphase obtained from NI Mapping are reliable, suggesting the great potential for NI Mapping to reveal mechanical properties of the wood-adhesive interphase.

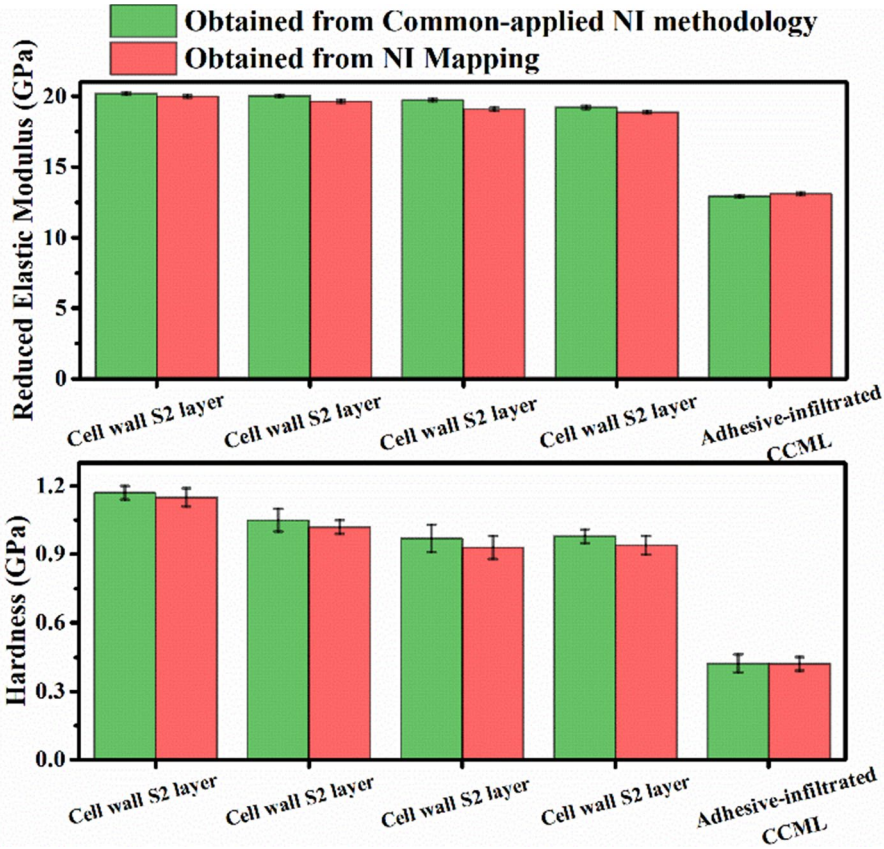


**Fig. 3** Comparison between the elastic modulus and hardness of cell wall S2 layer and CCML obtained from NI Mapping and the commonly applied NI methodology. The error bars represent the corresponding variance of data sets

### Distribution of mechanical properties in the wood-adhesive interphase

As displayed in Figs. 4 and 5, NI Mapping can provide insights into the mechanical properties of the wood-adhesive interphase in large scale ($100 \times 100$ μm$^2$). Benefiting from the large amounts of conducted indents ($100 \times 100$ indents), the obtained cartography of elastic modulus of wood-adhesive interphase exhibits high resolution compared with the one obtained from previous research (Konnerth et al. 2007; Li et al. 2017; Zhang et al. 2020). Moreover, the variation in the mechanical properties of adhesive, cell wall and CCML is obvious.

Due to the large-scale and high-resolution visualization achieved by NI Mapping, the correlation between adhesive infiltration and mechanical properties of the wood-adhesive interphase can be well-revealed. Herein, the distribution of mechanical properties in the two wood-adhesive interphases was investigated, i.e., wood-PF interphase and wood-PUR interphase. The investigation suggested that the adhesive

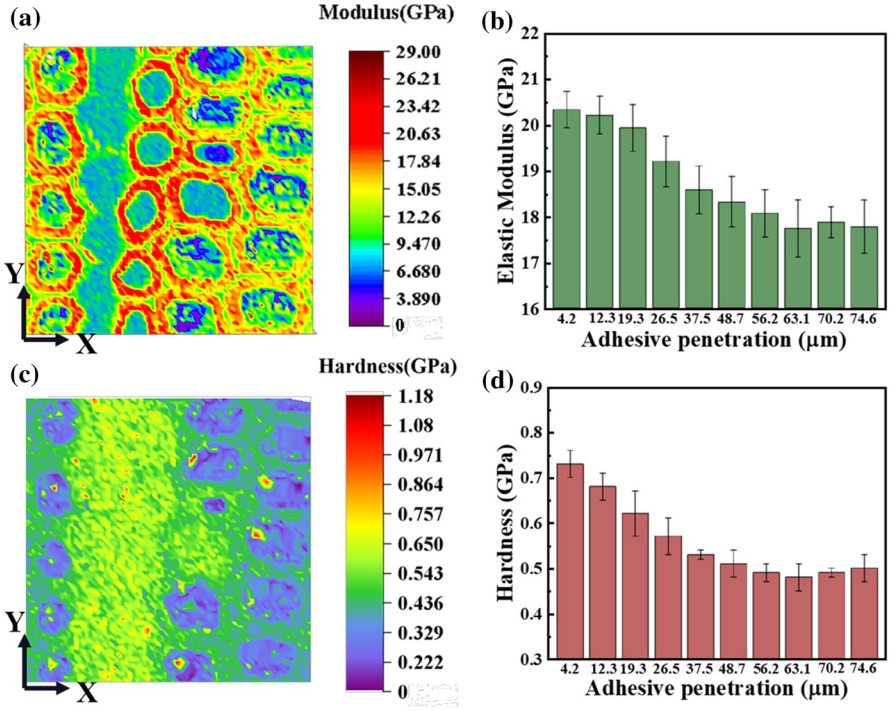


**Fig. 4** Cartographies of elastic modulus **a** and hardness **c** of wood-PF interphase with a dimension of 100 (Y)×100 (X) μm$^2$. The elastic modulus and hardness of cell wall S2 layer obtained from corresponding cartography are displayed in **b** and **d**, respectively

infiltration leads to the enhancement in elastic modulus and hardness of cell wall in the wood-adhesive interphase, which is in accordance with previous research (Konnerth et al. 2007; Liu et al. 2014). Figures 4 and 5 present the cartographies of elastic modulus and hardness of wood-PF and wood-PUR interphase, respectively. As displayed, elastic modulus and hardness of PF adhesive are 9.4 GPa and 0.79 GPa, respectively. The mechanical properties of the cell wall that directly contacts with PF adhesive are evidently elevated (20.4 GPa of elastic modulus and 0.67 GPa of hardness). It can be attributed to the infiltration of PF adhesive which can fill and interact with the cell wall skeleton (Wang et al. 2016, 2017b). IPNs formed between PF adhesive and cell wall can also be beneficial for elevating the mechanical properties of cell wall (Jakes et al. 2015).

Figure 4b and d further reveals a gradient distribution of mechanical properties corresponding to cell wall S2 layers in the wood-PF interphase as PF adhesive can infiltrate the wood substrate. The x-coordinates in Fig. 4b and d represent the adhesive infiltration depth (along the X direction) as measured from the glue line which is set as 0 μm, and the error bars represent the corresponding variance of data sets. As shown, the adhesive infiltration shows limitation in the enhancement of cell wall S2 layer as the infiltration of PF adhesive exceeds 60 μm. It can

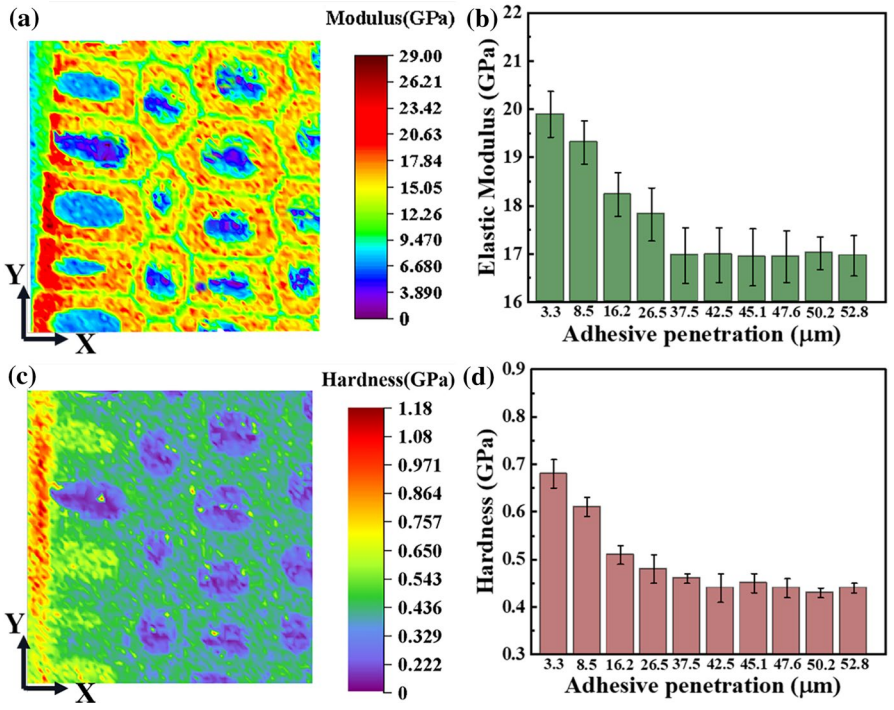


**Fig. 5** Cartography of reduced elastic modulus **a** and hardness **c** of wood-PUR interphase with a dimension of 100 (Y) × 100 (X) $\mu m^2$. The elastic modulus and hardness of cell wall S2 layer obtained from corresponding cartography are displayed in **b** and **d**, respectively

be attributed to the limited infiltration of PF adhesive in cell wall S2 layer that was located far from the glue line.

Figure 5 reveals the significant variation in the mechanical properties of wood-PUR interphase as compared with the wood-PF interphase. The variations can be well-explained by the differences in the infiltration behavior relating to the two selected adhesives. As shown in Fig. 5a and c, the elastic modulus and hardness of PUR are weaker compared with the PF adhesive (8.2 GPa of elastic modulus and 0.53 GPa of hardness). The limited infiltration of PUR in the cell wall is also well-revealed by Fig. 5. The mechanical properties of cell wall S2 layer that directly contacts with PUR adhesive are 19.8 GPa of elastic modulus and 0.64 GPa of hardness, respectively. The comparably large molecule size of the PUR can significantly hinder its infiltration into the cell wall, which further leads to the limited mechanical properties of the cell wall (Herzele et al. 2020). However, as indicated by previous literature (Gindl et al. 2004; Liu et al. 2018), PUR adhesive seems to be unlikely to infiltrate into cell wall S2 layer. In this work, the obvious enhancement of mechanical properties of cell wall S2 layer in wood-PUR interphase was found, indicating that only limited amount of PUR infiltrated the cell wall. This finding can be attributed to the fact that the major reactive compounds

in PUR are isocyanates, which may react with the cellulosic skeleton (Kläusler et al. 2014; Wang et al. 2018b). As reported, isocyanates can penetrate into the wood cell wall and further lead to the enhanced mechanical properties of cell wall S2 layer. It should also be noted that the formula of adhesive can affect the infiltration significantly and the PUR adhesive used in this work exhibits a low viscosity (300 mPa·s). Thus, the corresponding results might only be suitable for the PF and PUR adhesive used in this work.

Comparison between the cartographies obtained from NI Mapping of wood-PF and wood-PUR interphases revealed a weaker wood-PUR interphase than wood-PF interphase, which can be attributed to the limited infiltration of PUR adhesive into the cell wall. The X-coordinate in Fig. 5b and d represents the adhesive infiltration depth (along X direction) as measured from the glue line which is set as 0 μm, and the error bars represent the corresponding variance of data sets. Figure 5c and d shows that enhancement in cell wall S2 layer as induced by PUR infiltration exhibited a limitation as the infiltration depth of PUR adhesive exceeded 30 μm. This result further verifies the limited infiltration depth of PUR adhesive.

## Mechanical properties of early wood-adhesive interphase

The obtained results clearly suggested the correlation between adhesive infiltration and the enhanced mechanical properties of the wood-adhesive interphase. However, limited size of wood-PUR interphase was observed, and it may lead to concentration of stress and strain according to previous research (Gindl et al. 2005, Serrano et al. 2005). The concentration of stress and strain can result in the slipping deformation and rupture of wood-PUR interphase (Li et al. 2017). Figure 6a and b shows the shearing strength of wood-PF and wood-PUR bonds. The shear strength corresponding to wood-PF bonds is 5.2 MPa, which exhibits advantages against the ones of wood-PUR bonds (4.3 MPa). It can be attributed to the significant variation in the mechanical properties of two wood-adhesive interphases induced by different infiltration behaviors. Limited infiltration of PUR adhesive and comparably weaker mechanical properties of wood-PUR interphase led to the concentration of stress and strain. Thus, wood-PUR bonds exhibit weaker macro-mechanical properties as compared with the wood-PF bonds.

Further investigation into the fracture of wood-PF interphase revealed that the fracture of early wood-adhesive interphase occurs before that of late wood-PF interphase. It can be attributed to the poor lignification, low density and disordered microfibril arrangement of the early wood (Li et al. 2019). As displayed in Fig. 6c and d, optical image reveals the evident fracture of the early wood-PF interphase after shearing tests, emphasizing the importance of revealing the mechanical properties of early wood-adhesive interphase. However, the relevant research is rather limited due to the fact that the thickness of the cell wall in early wood is insufficient for the commonly applied NI analysis. NI Mapping was hereby applied to reveal the mechanical properties of early wood-PF interphase aiming for comprehensively investigating the mechanical properties of the

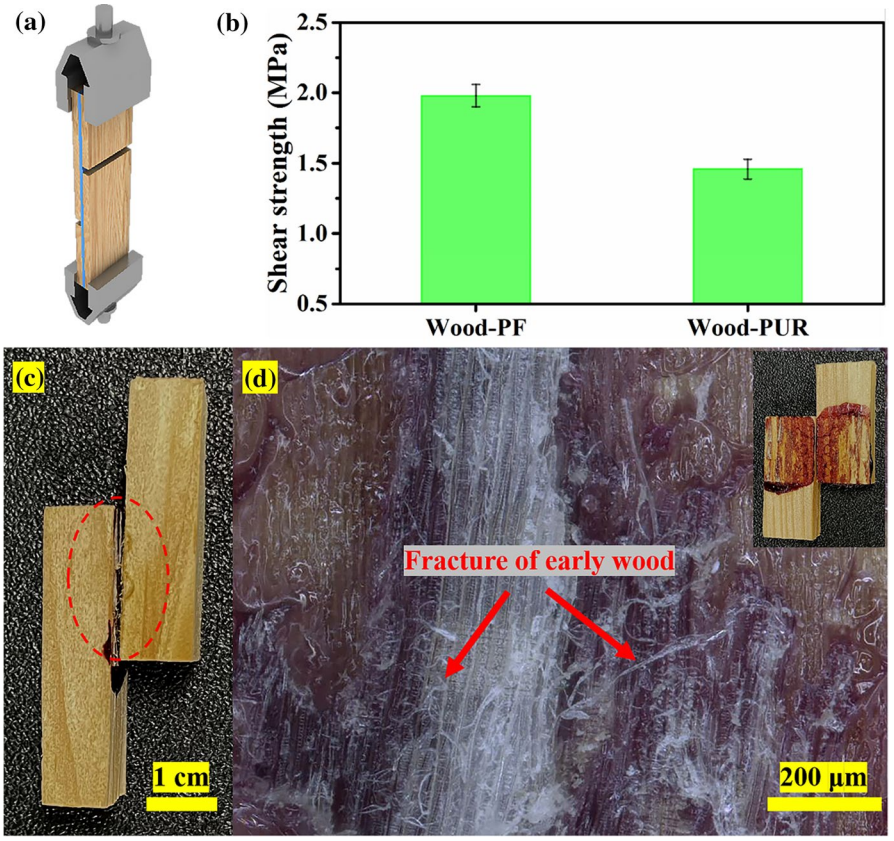


**Fig. 6** **a** Schematic diagram of testing the shearing strength of wood-adhesive bonds. **b** Shearing strength of wood-PF and wood-PUR bonds. **c–d** Optical image of fracture mode of wood-PF bonds and the fracture of early wood-adhesive interphase after shearing tests.

wood-adhesive interphase (Fig. 7). Glue line in the early wood-PF interphase is indistinctive as compared with the one in the late wood-PF interphase. This finding can be attributed to the elevated capillarity of early wood due to the large lumen (Wascher et al. 2020). Results obtained from NI Mapping revealed that the mechanical properties of cell wall in early wood can be elevated by PF adhesive infiltration. The elastic modulus and hardness of cell wall in early wood-PF interphase are 17.5 GPa and 0.65 GPa, respectively, which is still lower than the ones corresponding to the late wood-PF interphase. Meanwhile, Fig. 7c reveals the elevation of mechanical properties of the cell wall in the early wood-adhesive interphase reaches limitations as infiltration of PF adhesive exceeded 90 µm in early wood. Large amount of PF adhesive infiltrates into the lumen and it contributes to mechanical properties by mechanical interlock. The pristine

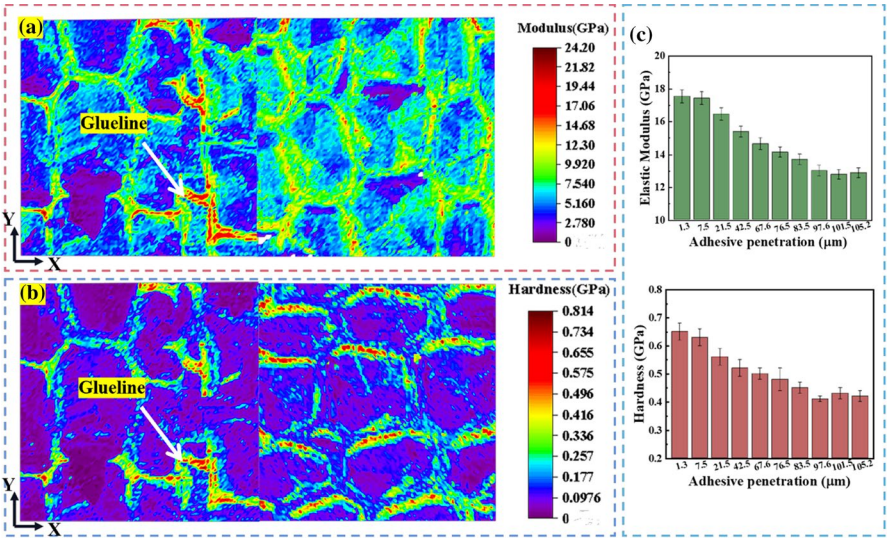


**Fig. 7** Cartography of reduced elastic modulus **a** and hardness **b** in the early wood-PF interphase with a dimension of 100 (Y) × 200 (X) $\mu m^2$. **c** Elastic modulus and hardness of cell wall obtained from the cartographies and the X-coordinates represent the adhesive infiltration depth. The error bars represent the corresponding variance of data sets

mechanical properties of early wood are lower than those of late wood leading to the damage begin from the early wood-PF interphase.

## High-efficiency of NI mapping

NI Mapping reported in this work caves a promising way for large-scale and high-resolution visualization of wood-adhesive interphase, which provides insights into establishing the correlation between adhesive infiltration and mechanical properties of the wood-adhesive interphase. The obtained results are reliable compared with commonly applied NI methodology. In addition, the time consumed for achieving NI Mapping is approximately 180 min when a total amount of 100 × 100 indents is conducted. As compared with commonly applied NI methodology (~ 20 s for single indent and total time more than 3300 min for 100 × 100 indents), NI Mapping exhibits advantages in terms of time-saving and high-efficiency. As listed in Table 1, NI Mapping can be applied to reveal the distribution of mechanical properties on material surface in a large scale. Due to the fact that a minimum indent spacing should be 5–7 times of indent depth, the resolution for NI Mapping on wooden materials exhibits limitation (Cao et al. 2021). The resolution proposed in this work has approached the aforementioned limitation and it also is with reliable accuracy and high-efficiency.

**Table 1** Summarization of relevant research based on nanoindentation mapping

| AOI[a] | Resolution[b] | Scale (μm$^2$) | Method | Ref. |
|---|---|---|---|---|
| Fiber-epoxy interphase | 5 × 15 | 20 × 30 | Common-applied NI methodology | Li et al. (2017) |
| Wood-adhesive interphase | 18 × 45 | 17 × 90 | Common-applied NI methodology | Konnerth et al. (2007) |
| Thermal barrier coating | 50 × 75 | 50 × 75 | NI Mapping | Vignesh et al. (2019) |
| Titanium alloys | 50 × 400 | 50 × 100 | NI Mapping | Liu et al. (2021) |
| Wood-coating interphase | 100 × 100 | 100 × 100 | NI Mapping | Wu et al. (2021) |
| Wood-adhesive interphase | 100 × 100 | 100 × 100 | NI Mapping | This work |

[a]area of interest

[b]The resolution is presented as the total amount of indents

## Conclusion

NI Mapping was used to reveal the mechanical properties of wood-adhesive interphase in large scale and high-resolution visualization. Comparison between the mechanical properties obtained from NI Mapping and commonly applied NI methodology revealed the variation is less than 3%, indicating the convincible reliability of NI Mapping. Total time for NI Mapping is 180 min indicating its advantages in terms of time-saving and high-efficiency. In addition, NI Mapping can be successfully applied to investigate the correlation between adhesive infiltration and mechanical properties of cell wall S2 layer in the wood-PF interphase and wood-PUR interphase. The obtained results confirmed the gradient distribution of the mechanical properties of the wood-adhesive interphase as adhesive infiltrating. Due to the smaller molecule size of PF adhesives, infiltration of PF adhesive into cell wall exhibits advantages compared with PUR adhesives. Compact IPNs as-induced by favored infiltration of PF adhesive in cell wall S2 layer improved the mechanical properties of the wood-PF interphase, which consequently resulted in elevated macro-mechanical properties (5.2 MPa of shear strength) of wood-PF bonds as compared with the wood-PUR interphase. Furthermore, NI Mapping can also be applied to well reveal the mechanical properties of early wood and the interphase formed by early wood and adhesives. This study clearly showed that NI Mapping is a potential and suitable way for large-scale and high-resolution visualization of mechanical properties of the wood-adhesive interphase.

**Supplementary Information** The online version contains supplementary material available at https://doi.org/10.1007/s00226-022-01394-x.

**Acknowledgements** The authors gratefully the funding support from the National Natural Science Foundation of China (31870548), the Research Foundation of Talented Scholars of Zhejiang A & F University (2020FR070).

## Declarations

**Conflict of interest** The authors declare no conflict of interest.

## References

Aicher S, Hirsch M, Christian Z (2016) Hybrid cross-laminated timber plates with beech wood cross-layers. Constr Build Mater 124:1007–1018

Altgen D, Grigsby W, Altgen M et al (2019) Analyzing the UF resin distribution in particleboards by confocal laser scanning microscopy. Compos Part A-Appl s 125:105529

Baldan A (2012) Adhesion phenomena in bonded joints. Int J Adhes Adhes 38:95–116

Beaulieu J, Dutilleul P (2019) Applications of computed tomography (CT) scanning technology in forest research: a timely update and review. Can J Forest Res 49(10):1173–1188

Cao Y, Zhang W, Yang P et al (2021) Comparative investigation into the interfacial adhesion of plywood prepared by air spray atomization and roller coating. Eur J Wood Prod 79(4):887–896

Evans P, Morrison O, Senden T et al (2010) Visualization and numerical analysis of adhesive distribution in particleboard using X-ray micro-computed tomography. Int J Adhes Adhes 30(8):754–762

Frihart R (2013) Wood adhesion and adhesives. Crc Press-Taylor & Francis Group, Boca Raton

Gindl S, Jeronimidis G (2004) The interphase in phenol–formaldehyde and polymeric methylene diphenyldiisocyanate glue lines in wood. Int J Adhes Adhes 24:279–286

Gavrilovic-Grmusa I, Dunky M, Miljkovic J et al (2012) Influence of the viscosity of UF resins on the radial and tangential penetration into poplar wood and on the shear strength of adhesive joints. Holzforschung 66(7):849–856

Gindl W, Sretenovic A, Vincenti A et al (2005) Direct measurement of strain distribution along a wood bond line. Part 2: Effects of adhesive penetration on strain distribution. Holzforschung 59(3):307–310

Herzele S, van Herwijnen G, Edler M et al (2018) Cell-layer dependent adhesion differences in wood bonds. Compos Part A-Appl s 114:21–29

Herzele S, van Herwijnen H, Griesser T et al (2020) Differences in adhesion between 1C-PUR and MUF wood adhesives to (ligno)cellulosic surfaces revealed by nanoindentation. Int J Adhes Adhes 98:102507

Huang Y, Yang Z, Ren W et al (2015) 3D meso-scale fracture modelling and validation of concrete based on in-situ X-ray Computed Tomography images using damage plasticity model. Int J Solids Struct 67–68:340–352

Jakes J, Frihart C, Hunt C et al (2019) X-ray methods to observe and quantify adhesive penetration into wood. J Mater Sci 54(1):705–718

Jakes J, Frihart R, Beecher F et al (2008) Experimental method to account for structural compliance in nanoindentation measurements. J Mater Res 23(4):1113–1127

Jakes J, Hunt G, Yelle J et al (2015) Synchrotron-based X-ray fluorescence microscopy in conjunction with nanoindentation to study molecular-scale interactions of phenol-formaldehyde in wood cell walls. ACS Appl Mater Interfaces 7(12):6584–6589

Jakes J, Stone D (2021) Best practices for Quasistatic Berkovich Nanoindentation of Wood Cell Walls. Forests 12(12):1696

Kamke F (2007) Adhesive penetration in wood—a review. Wood Fiber Sci 39(2):205–220

Kamke F, Nairn J, Muszynski L et al (2014) Methodology for micromechanical analysis of wood adhesive bonds using X-ray computed tomography and numerical modeling. Wood Fiber Sci 46(1):15–28

Kläusler O, Bergmeier W, Karbach A et al (2014) Influence of N, N-dimethylformamide on one-component moisture-curing polyurethane wood adhesives. Int J Adhes Adhes 55:69–76

Konnerth J (2014) Effect of plasma treatment on cell-wall adhesion of urea-formaldehyde resin revealed by Nanoindentation. Holzforschung 68(6):707–712

Konnerth J, Gindl W (2006) Mechanical characterisation of wood-adhesive interphase cell walls by nanoindentation. Holzforschung 60(4):429–433

Konnerth J, Valla A, Gindl W (2007) Nanoindentation mapping of a wood-adhesive bond. Appl Phys a: Mater Sci Process 88(2):371–375

Kutukova K, Niese S, Sander C et al (2018) A laboratory X-ray microscopy study of cracks in on-chip interconnect stacks of integrated circuits. Appl Phys Lett 113(9):091901
Li A, Jiang J, Lu J (2019) Differences in the viscoelastic properties between earlywood and latewood in the growth rings of Chinese fir as analyzed by dynamic mechanical analysis (DMA) in the temperature range between-120 degrees C and 120 degrees C. Holzforschung 73(3):241–250
Li Q, Li Y, Zhou L (2017) Nanoscale evaluation of multi-layer interfacial mechanical properties of sisal fiber reinforced composites by nanoindentation technique. Compos Sci Technol 152:211–221
Li W, Wang M, Cheng J (2020) Indentation hardness of the cohesive-frictional materials. Int J Mech Sci 180:105666
Li X, Bhushan B (2002) A review of nanoindentation continuous stiffness measurement technique and its applications. Mater Charact 48:11–36
Liu C, Zhang Y, Wang S et al (2014) Micromechanical Properties of the Interphase in Cellulose Nanofiber-reinforced Phenol Formaldehyde Bondlines. BioResources 9(3):5529–5541
Liu H, Shang J, Kamke F et al (2018) Bonding performance and mechanism of thermal-hydro-mechanical modified veneer. Wood Sci Technol 52(2):343–363
Liu Z, Zhang J, He B et al (2021) High-speed nanoindentation mapping of a near-alpha titanium alloy made by additive manufacturing. J Mater Res 36(11):2223–2234
McKinley P, Kamke F, Sinha A et al (2018) Analysis of adhesive penetration into wood using nano-X-Ray computed tomography. Wood Fiber Sci 50(1):66–76
Obersriebnig M, Konnerth J, Gindl-Altmutter W (2013) Evaluating fundamental position-dependent differences in wood cell wall adhesion using nanoindentation. Int J Adhes Adhes 40:129–134
Obersriebnig M, Veigel S, Gindl-Altmutter W et al (2012) Determination of adhesive energy at the wood cell-wall/UF interface by nanoindentation (NI). Holzforschung 66(6):781–787
Oliver W, Pharr G (1992) An improved technique for determing hardness and elastic-modulus using load and displacement sensing indentation experiments. J Mater Res 7(6):1564–1583
Oliver W, Pharr G (2004) Measurement of hardness and elastic modulus by instrumented indentation: Advances in understanding and refinements to methodology. J Mater Res 19(1):3–20
Phani P, Oliver W, Pharr G (2021) Measurement of hardness and elastic modulus by load and depth sensing indentation: improvements to the technique based on continuous stiffness measurement. J Mater Res 36(11):2137–2153
Qi D, Hu W, Xin K et al. (2020) In-situ synchrotron X-ray tomography investigation of micro lattice manufactured with the projection micro-stereolithography (P mu SL) 3D printing technique: Defects characterization and in-situ shear test. Compos Struct 252 (112710)
Serrano E, Enquist B (2005) Contact-free measurement and non-linear finite element analyses of strain distribution along wood adhesive bonds. Holzforschung 59:641–647
Singh A, Nuryawan A, Park B et al (2015) Urea-formaldehyde resin penetration into Pinus radiata tracheid walls assessed by TEM-EDXS. Holzforschung 69(3):303–306
Szewczykowski P, Skarzynski L (2019) Application of the X-ray micro-computed tomography to the analysis of the structure of polymeric materials. Polimery 64(1):12–22
Vignesh B, Oliver W, Kumar G et al (2019) Critical assessment of high speed nanoindentation mapping technique and data deconvolution on thermal barrier coatings. Mater Des 181:108084
Wang X, Chen X, Xie X et al (2018a) Effects of thermal modification on the physical, chemical and micromechanical properties of Masson pine wood (Pinus massoniana Lamb.). Holzforschung 72(12):1063–1070
Wang X, Zhao L, Deng Y et al (2018b) Effect of the penetration of isocyanates (pMDI) on the nanomechanics of wood cell wall evaluated by AFM-IR and nanoindentation (NI). Holzforschung 72(4):301–309
Wang X, Deng Y, Li Y et al (2016) In situ identification of the molecular-scale interactions of phenol-formaldehyde resin and wood cell walls using infrared nanospectroscopy. RSC Adv 6(80):76318–76324
Wang X, Wang S, Xie X et al (2017a) Multi-scale evaluation of the effects of nanoclay on the mechanical properties of wood/phenol formaldehyde bondlines. Int J Adhes Adhes 74:92–99
Wang X, Zhao L, Xu B et al (2017b) Effects of accelerated aging treatment on the microstructure and mechanics of wood-resin interphase. Holzforschung 72(3):235–241
Wascher R, Bittner F, Avramidis G et al (2020) Use of computed tomography to determine penetration paths and the distribution of melamine resin in thermally-modified beech veneers after plasma treatment. Compos Part A-Appl S 132:105821

Wimmer R, Lucas B (1997) Comparing mechanical properties of secondary wall and cell corner middle lamella in spruce wood. IAWA J 18(1):77–88

Wu Y, Zhang H, Yang L et al (2021) Understanding the effect of extractives on the mechanical properties of the waterborne coating on wood surface by nanoindentation 3D mapping. J Mater Sci 56(2):1401–1412

Yu Z, Fan M (2017) Short- and long-term performance of wood based panel products subjected to various stress modes. Constr Build Mater 156:652–660

Zauner M, Keunecke D, Mokso R et al (2012) Synchrotron-based tomographic microscopy (SbTM) of wood: development of a testing device and observation of plastic deformation of uniaxially compressed Norway spruce samples. Holzforschung 66(8):973–979

Zhang T, Bai S, Zhang Y et al (2012) Viscoelastic properties of wood materials characterized by nanoindentation experiments. Wood Sci Technol 46(5):1003–1016

Zhang X, Zhao Q, Wang S et al (2010) Characterizing strength and fracture of wood cell wall through uniaxial micro-compression test. Compos Part A-Appl s 41(5):632–638

Zhang Z, Cai S, Li Y et al (2020) High performances of plant fiber reinforced composites-A new insight from hierarchical microstructures. Compos Sci Technol 194:108151



## Authors and Affiliations

**Chuhang Xu[1] · Yizhong Cao[1,2] · Haili Chen[1,2] · Yujing Nie[1,2] · Yujie Meng[3] · Qiang Wu[1,2] · Siqun Wang[4]**

[1] College of Chemistry and Materials Engineering, Zhejiang A&F University, Hangzhou 311300, China

[2] National Engineering and Technology Research Center of Wood-Based Resources Comprehensive Utilization, Hangzhou 311300, China

[3] KLA Corporation, One Technology Drive, Milpitas, CA 95035, USA

[4] Center for Renewable Carbon, University of Tennessee, Knoxville, TN 37996, USA